Synthesis and Chemical−Pharmacological Characterization of the Antimetastatic NAMI-A-Type Ru(III) Complexes (Hdmtp)[*trans*-$RuCl_4$(dmso-S)(dmtp)], (Na)[*trans*-$RuCl_4$(dmso-S)(dmtp)], and [*mer*-$RuCl_3(H_2O)$(dmso-S)(dmtp)] (dmtp = 5,7-Dimethyl[1,2,4]triazolo[1,5-*a*]pyrimidine)

Aldrik H. Velders,*,† Alberta Bergamo,‡ Enzo Alessio,§ Ennio Zangrando,§ Jaap G. Haasnoot,† Claudia Casarsa,‡ Moreno Cocchietto,‡ Sonia Zorzet,|| and Gianni Sava‡,||

Leiden Institute of Chemistry, Gorlaeus Laboratories, Leiden University, P.O. Box 9502, 2300 RA Leiden, The Netherlands, Callerio Foundation-Onlus, Via A. Fleming 22-31, 34127 Trieste, Italy, Department of Chemical Sciences, University of Trieste, Via L. Giorgieri 1, 34127 Trieste, Italy, and Department of Biomedical Sciences, University of Trieste, Via L. Giorgieri, 34127 Trieste, Italy

Received August 4, 2003

Ruthenium compounds have gained large interest for their potential application as chemotherapeutic agents, and in particular the complexes of the type (X)[*trans*-$RuCl_4$(dmso-S)L] (X = HL or Na, NAMI-A or NAMI, respectively, for L = imidazole) are under investigation for their antimetastatic properties. The NAMI(-A)-like compounds are prodrugs that hydrolyze in vivo, and the investigation of their hydrolytic properties is therefore important for determining the nature of the potential active species. The NAMI-A-type Ru(III) complex **1**, (Hdmtp)[*trans*-$RuCl_4$(dmso-S)(dmtp)] (dmtp is 5,7-dimethyl[1,2,4]triazolo[1,5-*a*]pyrimidine), and the corresponding sodium analogue **2**, (Na)[*trans*-$RuCl_4$(dmso-S)(dmtp)], were synthesized. The hydrolyses of **1** and **2** in water as well as in buffered solutions were studied, and the first hydrolysis product, [*mer*-$RuCl_3(H_2O)$(dmso-S)(dmtp)]·H_2O (**3**), was isolated and characterized. The molecular structures of **1** and **3** were determined by single-crystal X-ray diffraction analyses and prove the importance of the hydrogen-bonding properties of dmtp to stabilize hydrolysis products. In vitro **1** (a) is not cytotoxic on tumor cells, following challenges from 1 to 72 h and concentrations up to 100 μM, (b) inhibits matrigel invasion at 0.1 mM and MMP-9 activity with an IC_{50} of about 1 mM, and (c) is devoid of pronounced effects on cell distribution among cell cycle phases. In vivo compound **1**, similar to NAMI-A, significantly inhibits metastasis growth in mice bearing advanced MCa mammary carcinoma tumors. In the lungs, **1** is significantly less concentrated than NAMI-A, whereas no differences between these two compounds were found in other organs such as tumor, liver, and kidney. However, **1** caused edema and necrotic areas on liver parenchyma that are more pronounced than those caused by NAMI-A. Conversely, glomerular and tubular changes on kidney are less extensive than with NAMI-A. In conclusion, **1** confirms the excellent antimetastatic properties of this class of NAMI-A-type compounds and qualifies as an interesting alternative to NAMI-A for treating human cancers.

Introduction

In the past decade, ruthenium complexes have gained large interest for their potential use as therapeutic anticancer agents.[1−4] Recently, several types of ruthenium(II) complexes with arene ligands[5,6] or heterocyclic bidentate ligands[7,8] have proven to have significant antitumor activity. However, best studied are ruthenium(III) complexes. In particular Keppler-type complexes (HL)[*trans*-$RuCl_4L_2$], with L a heterocyclic nitrogen ligand, have shown promising results on colorectal autochthonous tumors.[9−11] The related tetrachlororuthenium(III) dmso complexes of the type (X)[*trans*-$RuCl_4$(dmso-S)L] (X = HL or Na, NAMI-A or NAMI, respectively, for L = imidazole;[12,13] see Figure 1) are under investigation for their specific antimetastatic properties since the early 1990s and have shown interesting pharmacological properties in preclinical trials.[14−16] NAMI-A is the first ruthenium antitumor complex that has entered clinical testing and recently has successfully completed a phase I trial at the Netherlands Cancer Institute of Amsterdam.[17] Although the mechanism of action of the NAMI-A-type complexes (HL)[*trans*-$RuCl_4$(dmso-S)L] is not yet unraveled, they appear to be precursors that hydrolyze rapidly in vivo, forming a number of potentially active species.[18] The investigation of the hydrolytic properties of this type of complex is therefore important for determining the nature of the active species and is necessary for defining the protocols for the administration of the drugs.[19,20]

Because of their hydrogen-bonding properties, triazolopyrimidines are useful ligands for tuning the physi-

* To whom correspondence should be addressed. Current address: Molteni Farmaceutici, S.S. 67 Loc. Granatieri, I-50018 Scandicci, Florence, Italy. Phone: +39 055 7361330. Fax: +39 055 7361288. E-mail: a.velders@chem.leidenuniv.nl.
† Leiden University.
‡ Callerio Foundation-Onlus.
§ Department of Chemical Sciences, University of Trieste.
|| Department of Biomedical Sciences, University of Trieste.

10.1021/jm030984d CCC: $27.50
Published on Web 01/21/2004

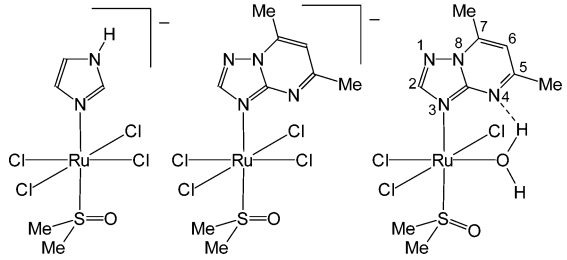

Figure 1. Structural representation of the anion of NAMI-(-A), left, the anion of **1** and **2**, middle, and their first hydrolysis product, **3**, right. The dmtp numbering scheme is also shown.

cochemical properties of metal ions and other coordinated ligands.[21,22] By use of the 5,7-dimethyl[1,2,4]triazolo-[1,5-*a*]pyrimidine ligand (dmtp; see Figure 1), it has been possible to synthesize, isolate, and characterize the first hydrolysis product of Keppler-type antitumor complexes,[3,10] namely, the aquatrichlororuthenium(III) complex [*trans*-$RuCl_3(H_2O)(dmtp)_2$]·H_2O.[23] In this complex, the dmtp ligands play a crucial role as they coordinate to the ruthenium(III) ion through their triazolic N(3) nitrogen atoms while the pyrimidinic N(4) nitrogen atoms stabilize the coordinated water molecule via double intramolecular hydrogen bondings.

In the search for new antitumor-active ruthenium complexes and in order to get a better understanding of the hydrolytic properties and products of NAMI(-A)-type compounds, analogous complexes with the dmtp ligand were prepared (Figure 1). In this paper, the synthesis and characterization of (Hdmtp)[*trans*-$RuCl_4$(dmso-S)(dmtp)] (**1**) and of (Na)[*trans*-$RuCl_4$(dmso-S)(dmtp)] (**2**) are presented. The hydrolytic properties of **1** and **2** were studied, and the first hydrolysis product of both compounds, [*mer*-$RuCl_3(H_2O)$(dmso-S)(dmtp)]·H_2O (**3**) (Figure 1), was isolated and characterized. The molecular structures of **1** and **3** were determined by single-crystal X-ray diffraction analysis; this is the first report of the complete structural characterization of a NAMI-A-type complex and its first hydrolysis product, in solution as well as in the solid state. Compound **1** was also examined in detail in vitro for cytotoxicity, invasion, and cell cycle effects and in vivo for tumor and metastasis inhibition and for host toxicity.

Results

Syntheses. The new tetrachlororuthenium(III) complexes (Hdmtp)[*trans*-$RuCl_4$(dmso-S)(dmtp)] (**1**) and (Na)-[*trans*-$RuCl_4$(dmso-S)(dmtp)] (**2**) are readily formed following the procedures previously reported for complexes of the type (HL)[*trans*-$RuCl_4$(dmso-S)(L)] and (Na)[*trans*-$RuCl_4$(dmso-S)(L)], respectively, L being a heterocyclic N ligand.[13,18,24] Whereas it appears very difficult to synthesize the anionic Keppler-type complex *trans*-$[RuCl_4(dmtp)_2]^-$ without obtaining impurities of the hydrolyzed complex [*trans*-$RuCl_3(H_2O)(dmtp)_2$]·H_2O,[25] the NAMI-(A)-type complexes **1** and **2** are relatively easily prepared, without impurities of hydrolysis products, e.g., **3**. Interestingly, attempts to prepare a NAMI-A analogue using acyclovir (acv) were unsuccessful and only the solvolyzed [*mer*-$RuCl_3(H_2O)$-(dmso-S)(acv)] species was obtained, also from nonaqueous solvent.[26]

Upon dissolution in aqueous solutions, complexes **1** and **2** hydrolyze (slowly) and the first hydrolysis product, [*mer*-$RuCl_3(H_2O)$(dmso-S)(dmtp)]·H_2O, **3**, is isolated as a crystalline precipitate. The main difference between these two synthetic routes to **3** is the final color of the solution from which the crystals separate. The light-orange color of a fresh solution of **2** gradually turns to yellow-brown and finally to green before crystals of **3** separate. This green color of the solution has been attributed to the concomitant formation of polymeric ruthenium oxo- and/or hydroxo-bridged species.[18,27] On the other hand, an aqueous solution of **1** is still light-orange a day after dissolution of the complex, and crystals of **3** precipitate therein. The lower pH (∼2) in the latter solution very likely prevents the formation of polymeric species.[24]

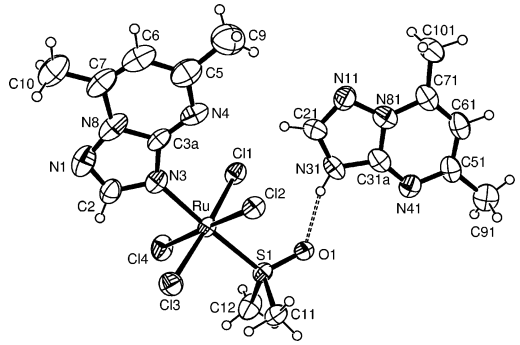

Figure 2. Molecular structure of (Hdmtp)[*trans*-$RuCl_4$(dmso-S)(dmtp)], **1**. The cocrystallized solvent molecule is omitted for clarity.

Characterization in Solid State and Solution. Complexes **1** and **3** were characterized in the solid state using single-crystal X-ray diffraction analyses, and all three complexes **1**−**3** were analyzed by infrared spectroscopy (IR; see Supporting Information). Below, the results are compared with those of related compounds, namely, NAMI, NAMI-A, and [*trans*-$RuCl_3(H_2O)(dmtp)_2$]·H_2O (from here on referred to as **4**). Complexes **1**−**3** were studied in solution using NMR and UV−vis spectroscopies. Complex **2** is insoluble in most organic solvents, as expected for a sodium salt. Remarkably, the Hdmtp salt **1**, like the neutral complex **3**, is rather soluble in some organic solvents such as dichloromethane.

X-ray diffraction analyses. The molecular structure of **1**, as derived from a single-crystal X-ray diffraction study, is shown in Figure 2. The anionic fragment exhibits an octahedral ruthenium(III) ion coordinated by four chloride ions in a plane and by a dmso and dmtp molecule in mutual trans positions. As in related complexes, the dmso is coordinated via the sulfur atom,[13,26,28] while the dmtp is coordinated via the N3 nitrogen.[23,25,29,30] The metal−ligand bond lengths of **1** are comparable to those of the related structures of NAMI[13] and NAMI-A,[31] as shown in Table 1. The Ru−dmtp bond is slightly longer, and correspondingly the Ru−dmso bond is slightly shorter with respect to the values detected in the imidazole complex. As a consequence, the dmso in **1** is more strongly bound to the Ru(III) ion than in NAMI(-A). Conversely, dmtp is more weakly bound in **1** than in the bis(dmtp) compound **4**. The cation in **1** is a protonated dmtp molecule at the N3 position, which is the most basic site.[21] The acidic hydrogen of the Hdmtp cation shows a strong hydrogen

Table 1. Metal−Ligand Distances (Å) of **1** and **3** in Comparison with Those of (Na)[*trans*-$RuCl_4$(DMSO)(Im)] (NAMI), (HIm)[*trans*-$RuCl_4$(dmso-S)(Im)] (NAMI-A), and [*trans*-$RuCl_3(H_2O)(dmtp)_2]\cdot H_2O$ (**4**) and Details of Intramolecular H-Bonding

	1	NAMI[13]	NAMI-A[31]	**3**	**4**[23,a]
Ru−N(3), Å	2.121(8)	2.081(2)	2.099(5)	2.137(2)	2 × 2.092(4)
Ru−S(1), Å	2.255(2)	2.296(1)	2.293(1)	2.267(1)	
Ru−Cl(1), Å	2.349(2)	2.340(1)	2.351(1)	2.332(1)	2.388(2)
Ru−Cl(2), Å	2.329(2)	2.323(1)	2.353(2)	2.313(1)	2.331(2)
Ru−Cl(3), Å	2.346(3)	2.359(1)	2.348(1)	2.337(1)	2.306(2)
Ru−Cl(4), Å	2.364(3)	2.345(1)	2.358(2)		
Ru−O(2), Å				2.094(2)	2.101(4)
O(2)···N(4), deg				2.707(2)	2.706(4)
O(2)···H−N(4), deg				149.4(3)	152(3)

[a] The $RuCl_3(H_2O)$ fragment lies on a crystallographic symmetry plane, thus relating the two dmtp ligands.

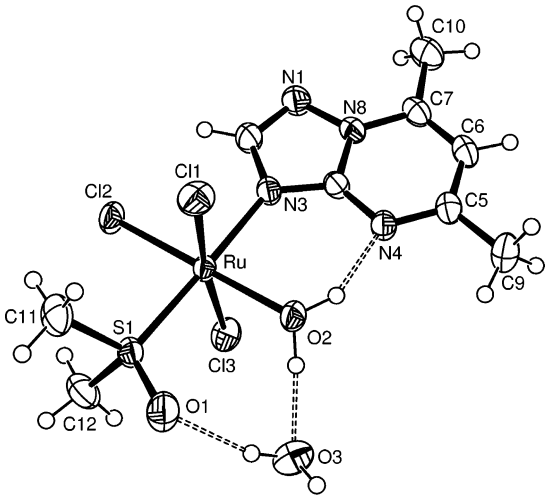

Figure 3. Molecular structure of [*mer*-$RuCl_3(H_2O)$(dmso-S)-(dmtp)], **3**. The intramolecular hydrogen bond between the coordinated water molecule and the pyrimidine nitrogen is indicated with a dashed line (O2···N4 is 2.707 Å).

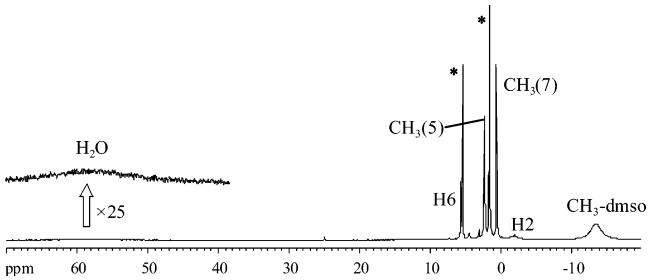

Figure 4. ^{1}H NMR spectrum of [*mer*-$RuCl_3(H_2O)$(dmso-S)-(dmtp)], **3**, in CD_2Cl_2. The residual solvent peaks (CH_2Cl_2 and H_2O) are marked with asterisks.

bond with the oxygen atom of the coordinated dmso molecule (N···O, 2.819 Å; N−H···O, 166°).

The molecular structure of **3** (Figure 3) shows a neutral ruthenium(III) complex in which the metal ion is octahedrally coordinated by three chloride ions in a mer configuration, one sulfur-bonded dmso molecule and a dmtp in mutual trans positions and a water molecule completing the coordination sphere. The metal−ligand distances are given in Table 1 in comparison with the data for **1** and **4**.[23] The Ru−S bond in **3** is slightly longer than in **1** but still significantly shorter than in NAMI and NAMI-A. In **3** the dmtp is involved in an intramolecular hydrogen bond via the pyrimidinic N4 nitrogen with a hydrogen of the coordinated water molecule (O2···N4, 2.707 Å; O2−H···N4, 149°). The hydrogen bond pattern is similar to that found in **4**,[23] and in [*trans*-$RuCl_3(H_2O)(admtp)_2]\cdot H_2O$ (admtp = 2-amino-dmtp),[29] although in **3** only one hydrogen atom of the water molecule is involved in an intramolecular hydrogen bond. In the structures of the related acyclovir (acv) and 9-ethylguanine (9Etg) complexes, [*mer*-$RuCl_3$(acv)-(dmso-S)$(H_2O)]\cdot H_2O$[26] and [*mer*-$RuCl_3$(9Etg)(dmso-S)-$(H_2O)]\cdot H_2O$,[28] respectively, the coordinated water molecule is involved in intramolecular hydrogen bonding with (the oxygen of) the heterocyclic ligand and also with the oxygen of the dmso. In the solid-state structure of **3**, even though the water and the dmso ligands are positioned in a way similar to that found in the above acyclovir and 9-ethylguanine structures, the dmso oxygen and the coordinated water are slightly too distant for hydrogen bonding (O···O, ∼3.1 Å). Actually, in the solid-state one hydrogen of the coordinated water molecule and the oxygen of the dmso are involved in an intermolecular hydrogen-bond network (see Supporting Information).

^{1}H NMR Spectrometry. The paramagnetic ruthenium(III) ion severely shifts and broadens the NMR signals of coordinated ligands, not allowing a standard assignment procedure. However, ^{1}H NMR data of complexes **1**−**3** were obtained, and assignment of most of the resonance peaks was done by comparison with related Ru(III)−dmso and Ru(III)−dmtp complexes.[13,23,25]

The ^{1}H NMR spectrum of **3** in CD_2Cl_2 (Figure 4) shows a large frequency range in which resonances are observed. The proton resonances of **3** were recognized using the inversion recovery pulse sequence and T_1 relaxation measurements to unambiguously discriminate the resonances of the paramagnetic compound (T_1 < 100 ms) from residual solvent peaks. A characteristic broad peak of the S-coordinated dmso is observed at −14 ppm,[13,18] and the resonances between +6 and −4 ppm are attributed to the dmtp protons.[23,25] Most characteristic is the very broad peak of the coordinated water molecule at about +60 ppm. This dramatic downfield shift for the proton resonances of a water molecule coordinated on a ruthenium(III) ion agrees well with what is found in related complexes such as **4** and [*trans*-$RuCl_3(H_2O)(admtp)_2]\cdot H_2O$.[23,25,29]

A fresh solution of **1** in deuterated water consists most likely of the anion [*trans*-$RuCl_4$(dmso-S)(dmtp)]$^-$ and the cation Ddmtp (the acidic proton of Hdmtp will rapidly be substituted by the excess of deuterium ions in D_2O). In fact, in the spectrum of **1** in D_2O, besides the severely broadened and shifted resonances of the paramagnetic anion, the sharp signals of the diamagnetic cation are also observed in the normal region (δ = 0−10). In dichloromethane it is unlikely that **1** is present in an ionic form, but probably represents a kind of ion pair stabilized by hydrogen bonding of the acidic

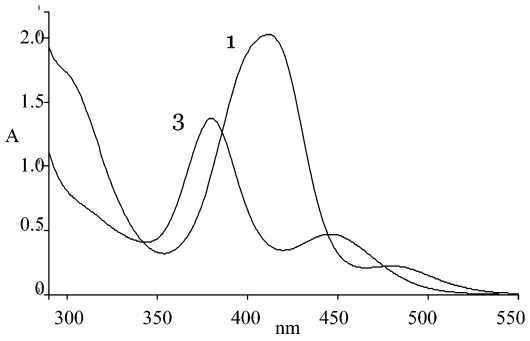

Figure 5. UV−vis absorption spectra of **1** (4.4×10^{-4} M) and **3** (4.8×10^{-4} M), both in CH_2Cl_2.

proton of the cation Hdmtp with the dmso of the anion (see Figure 2). This is in fact in accordance with the inversion recovery NMR experiments in which the proton resonances of the cation show relatively short T_1 times (<100 ms), indicating proximity of the resonating atoms to the paramagnetic ruthenium ion.

UV−Visible Spectroscopy. In the UV−vis absorption spectrum of **1** in dichloromethane (Figure 5) two distinct absorption bands in the visible region of the spectrum are observed, at 410 and 477 nm. The high-energy band is roughly a factor 8 more intense than the latter and has been attributed to a charge transfer (CT) band from the four coplanar chlorides to Ru.[32] In Figure 5 the absorption spectrum of compound **3** is also shown. Two clear absorption bands in the UV−vis (380 and 445 nm) are present; the Cl → Ru CT band is less intense than in the spectrum of **1** and is typical for three coordinated chloride ions in meridional geometry. With respect to the spectrum of **1**, both absorption bands of **3** are blue-shifted by about 30 nm.

Hydrolysis of 1 and 2 in Aqueous Solutions. It is important to have a good understanding of the hydrolysis of NAMI(-A)-type complexes in both buffered (pH 7.4) and nonbuffered (acidic) solutions.[19] Hydrolysis studies under physiological conditions yield information concerning the mechanism of action of the compound. However, prior to administration, which occurs through slow infusion, NAMI-A is dissolved in an acidified aqueous solution (pH ∼3) for stability reasons,[19,20] and thus, the hydrolysis studies under slightly acidic conditions are informative for that aspect. Although the hydrolysis of NAMI(-A)-type complexes can be measured by ^{1}H NMR spectrometry, the UV−vis absorption data are more readily monitored for practical reasons, especially when using buffered solutions.

The absorption spectrum of freshly dissolved **1** (or **2**) in water is similar to that in dichloromethane with an intense absorption band at 395 nm, (Ru → Cl CT) and an approximately 6 times less intense absorption at lower energy (460 nm). Interestingly, in the first hour after dissolution of **1** (or **2**) in water at 20 °C, the Ru → Cl CT absorption increases slightly (ca. 5%; Figure 6, top) accompanied by a 10 nm red shift of the absorption maximum, vide infra. Consecutively, in the course of a day, a slow but steady decrease of the main UV−vis absorption band is observed (Figure 6, bottom), and this is attributed to the hydrolysis of a chloride because the final spectrum with an absorption maximum at 365 nm (after 2 days) is very similar to that of **3** in dichloromethane (Figure 5). This hydrolysis is accompanied

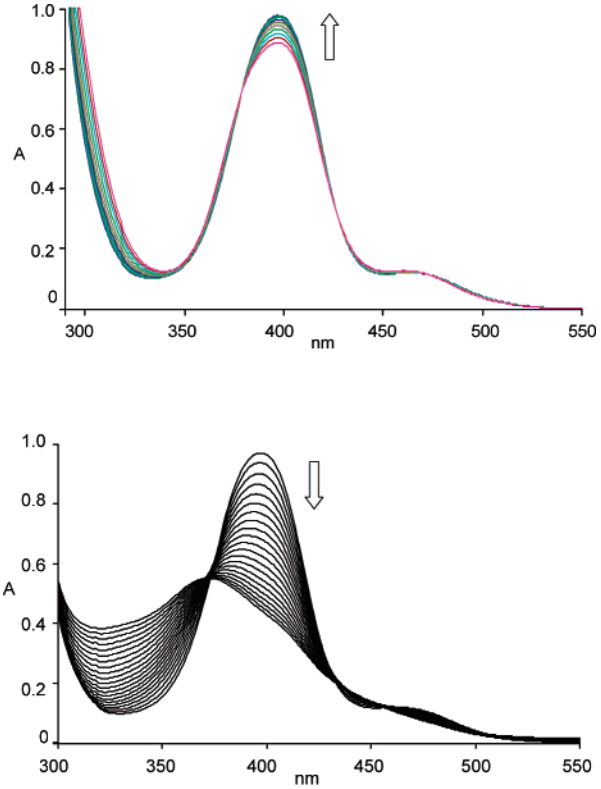

Figure 6. Time-dependent UV−vis absorption spectra of **1** in water (3.0×10^{-4} M) at 20 °C recorded every 2.5 min for 1 h (top) and consecutively recorded every 100 min (bottom).

by a lowering of the pH (from pH ∼7 to pH ∼3 in about a day). No further spectral changes are observed in the course of 2 days, not with UV−vis or with NMR measurements. Indeed, during this time interval, crystals of **3** formed from more concentrated solutions of either **1** or **2**.

We already mentioned the small increase of the Cl → Ru CT absorption in the first hour after dissolution of **1** in nonbuffered aqueous solutions (Figure 6, top). This observed increase is independent of the cation ($Hdmtp^+$ or Na^+) in the complex because it is observed for both **1** and **2**. The initial increase in absorption is not due to the slow dissolution of the compound, because in that case a steady increase of the whole absorption spectrum would be expected, while instead neat isosbestic points are observed. Although this increase of the Cl → Ru absorption has not been observed for NAMI(-A), some NAMI-A-type complexes do show a similar behavior as observed for **1** and **2**.[33] In the first hour after dissolution of **1** in D_2O, with NMR spectrometry, a decrease of the initial Ru(III)−dmtp signals is observed while new (paramagnetically shifted) dmtp and dmso signals appear, as expected for the hydrolysis of a chloride ion from **1**. Furthermore, an increase of the noncoordinated dmtp signals is observed; interestingly, no formation of noncoordinated dmso is observed. According to these NMR data, we attribute the initial increase in intensity of the absorption maximum with UV−vis spectroscopy to the partial release of the coordinated dmtp to form the [*trans*-$RuCl_4(dmso)(H_2O)]^-$ species, perhaps at equilibrium.

In physiological buffered solutions (PBS, pH 7.4), the hydrolysis of **1** and **2** is quite different from that observed in nonbuffered solutions (see Supporting In-

formation). First of all, at 20 °C the first hydrolysis step at pH 7.4 is much faster than the hydrolysis observed at slightly acidic pH ($t_{1/2} \approx 10$ min). Consecutively, a second hydrolysis step also occurs with a $t_{1/2}$ of about 1 h. Finally, in the course of a day, a very broad absorption band in the red region of the spectrum develops, corresponding to the observed green color of the solution. The first hydrolysis step at physiological pH is characterized by a shift of the main absorption band from 395 to 350 nm, which is similar to that observed for hydrolysis in nonbuffered solutions, vide supra (Figures 5 and 6), strongly indicating the first step to be the hydrolysis of a chloride ion. The second hydrolysis step at physiological pH is characterized by a further shift of the main absorption band from 350 to 320 nm and a decrease in intensity. The similarity of the first and second hydrolysis steps suggests the latter to be the hydrolysis of a chloride too. Finally, the appearance of a dark color is attributed to the (partial) formation of polymeric oxo-bridged species. The hydrolysis steps observed for **1** and **2** as followed with UV−vis absorption spectroscopy are remarkably similar to what is observed for NAMI(-A) under physiological conditions, in particular with regard to the shifts in absorption maxima.[13] The main difference with NAMI(-A) is that the first two hydrolysis steps of **1** and **2** occur more quickly.

The neutral compound **3** is poorly soluble in water at low pH but slightly soluble in buffered (pH ∼7) aqueous solutions. The UV−vis spectrum of a fresh solution of **3** in PBS shows an intense absorption peak at 350 nm and a pronounced shoulder at 415 nm. In the course of an hour after dissolution, the main peak decreases in intensity and a new absorption maximum at 320 nm is formed. This hydrolysis step is very similar to the second hydrolysis step observed for **1** in PBS and is characterized by a neat isosbestic point at 335 nm.

In summary, under nonbuffered, i.e., slightly acidic, conditions, a clear hydrolysis step is observed for **1** and **2**, the hydrolysis of a chloride ion to form the neutral compound [*mer*-$RuCl_3(H_2O)$(dmso-S)(dmtp)], **3**. At physiological pH, **1** and **2** also show a second hydrolysis step. Apparently, the neutral aqua compound [*mer*-$RuCl_3(H_2O)$(dmso-S)(dmtp)] does not hydrolyze further, but the hydroxo species [*mer*-$RuCl_3$(OH)(dmso)(dmtp)]$^-$ present at neutral pH does hydrolyze to form consecutive aquated species, like $[RuCl_2(H_2O)_2$(dmso)(dmtp)]$^+$ and $[RuCl_2$(OH)(H_2O)(dmso)(dmtp)]. The dmso is not released from **1** and **2** in the first hours after dissolution, neither in pure water nor at physiological pH. Prolonged storage at physiological pH, however, also induced the progressive release of dmtp and dmso. The details of these reactions are the subject of further investigation.

Solvolysis of 1 and 3 in Coordinating Solvents. In nonbuffered aqueous solutions, the partial release of dmso from NAMI-A is observed, which however can be delayed by addition of 5% dmso. In the first hour after dissolution of **1** in a mixture of water−dmso (90%/10%), a phenomenon is observed similar to what is found on dissolving **1** in nonbuffered water (see Figure 5, top); i.e., the absorption maximum at 400 nm gradually increases about 5% in intensity. Therefore, this result suggests that the observed spectral changes for **1** are not due to the release of dmso from **1**, which is furthermore consistent with the results from the NMR experiments in pure D_2O.

As observed for the complexes **4** and [*trans*-$RuCl_3(H_2O)(admtp)_2$],[23,25,29] time-dependent ^{1}H NMR and UV−vis spectroscopy and conductivity measurements of **3** in coordinating solvents (Solv = dmso, acetonitrile) indicate substitution of the coordinated water molecule by a solvent molecule, resulting in the formation of neutral trichlororuthenium(III) complexes of the type [*mer*-$RuCl_3$(Solv)(dmso-S)(dmtp)] in the course of a few hours at room temperature.[34]

Table 2. In Vitro Cytotoxicity of **1** on TS/A Adenocarcinoma, on KB Oral Carcinoma, and on B16-F10 Melanoma Cell Lines[a]

	exposure time [h]	concentration of **1** [μM]		
		1	10	100
TS/A	1 + 24	111 ± 16	65 ± 10	71 ± 3
	24	100 ± 1	93 ± 6	94 ± 4
	48	91 ± 2	96 ± 9	90 ± 6
	72	94 ± 1	99 ± 3	83 ± 3
KB	24	107 ± 6	102 ± 4	103 ± 7
	72	108 ± 12	97 ± 2	89 ± 2
B16-F10	24	78 ± 1*	64 ± 7**	78 ± 7*
	72	108 ± 12	94 ± 3	93 ± 2

[a] TS/A, KB, and B16-F10 cells, sown 24 h earlier, were treated with the compound at the indicated concentrations for the indicated time in complete medium supplemented with 5% of fetal calf serum. TS/A cells were also treated with compound dissolved in PBS for 1 h (1 + 24). Cell viability was evaluated by MTT assay at the end of each treatment or 24 h after the 1 h treatment in PBS. Each value is expressed as a percentage of the optical density of treated cells versus controls (% T/C) ± SE, calculated from the average of five separate wells. Statistical analysis includes ANOVA and Dunnett post-test ((*) $p < 0.05$ and (**) $p < 0.01$ vs controls).

Effects on Cell Viability. The effects of **1** on tumor cell proliferation were investigated on murine (TS/A adenocarcinoma and B16−F10 melanoma) and on human (KB oral carcinoma) cell lines. Table 2 reports the data of the effects on cell viability after treatment at 1, 10, or 100 μM for 1−72 h. The effects on the murine TS/A adenocarcinoma and on the KB human carcinoma cell line showed no change of cell proliferation at any concentration and at any time of analysis. Only murine B16-F10 melanoma cells showed a 30% inhibition of cell proliferation, dependent on the concentration being tested, after a 24 h challenge; the prolongation of treatment to 72 h showed loss of efficacy.

Inhibition of Tumor Cell Invasion and of MMP-9 Gelatinase. The capacity of **1** to inhibit tumor cell invasion, a fundamental step of the mechanism of tumor dissemination and metastasis, was tested by using a modified Boyden's chamber coated with matrigel and by determining the inhibition of gelatinolitic activity of MMP-9 by a zymography test (Figure 7 and inset). The inhibition of the enzymatic activity of MMP-9 in vitro is dose-dependent with an IC_{50} of approximately 0.6 mM. In the invasion test on modified Boyden's chamber, **1** is able to reduce to 27% the number of TS/A cells that invade the matrigel barrier.

Effects on Cell Cycle and Ruthenium Cell Uptake. The effects on cell distribution among cell cycle phases, following treatment with 100 μM **1** for 1 h, are reported in Figure 8. The effects were analyzed at 24 and 48 h after treatment to allow the phenomenon to

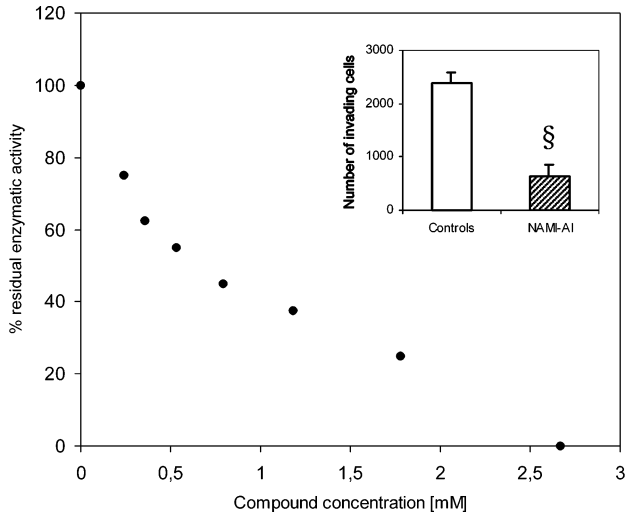

Figure 7. In vitro inhibition of gelatinase activity of MMP-9 and in vitro invasion by TS/A cells through matrigel-coated polycarbonate filters by **1**. Effect of **1** on MMP-9 gelatinase activity was evaluated from a densitometric scan of bands resulting from an SDS/polyacrylamide/gelatin gel loaded with culture medium of HT-1080 fibrosarcoma cells and treated with the compound at doses from 0.24 to 2.67 mM. As positive control, 10 mM EDTA was used. Histograms in the inset show the number of invading cells through a matrigel barrier. Statistical analysis results are the following: (§) $p = 0.0001$, extremely significant (unpaired t test).

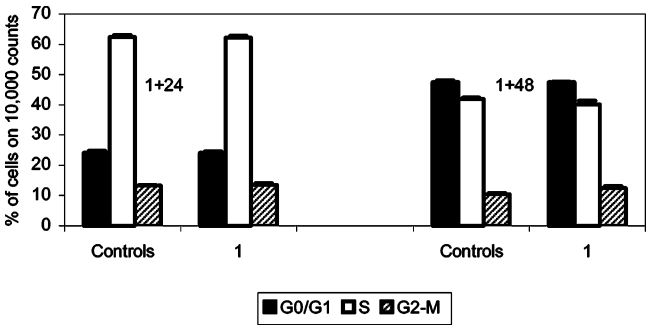

Figure 8. Effects of **1** on cell cycle distribution of murine TS/A adenocarcinoma cells. TS/A cells, sown 24 h earlier, were treated with the compound at 100 μM for 1 h in PBS. Cell cycle distribution was evaluated by flow cytometry after propidium iodide staining at 24 or 48 h. Data are calculated for experiments performed in triplicate.

be expressed. At any time of evaluation, no modification of the distribution of cells among cell cycle phases is evident. In the same samples the amount of ruthenium at the end of treatment, as measured by atomic absorption spectroscopy, is 0.408 ± 0.070 μg/10^6 cells (corresponding to about 4 nmol/10^6 cells, i.e., approximately a billion molecules of metabolites of **1** per cell); 24 h after the end of treatment, the amount of metabolites of **1** still present in tumor cells is approximately 54% (0.224 ± 0.028 μg/10^6 cells) of the amount measured immediately after the end of treatment. This result is consistent with a retention of ruthenium complex by tumor cells, and the dilution is imputable to the doubling of cell number in the 24 h following the end of treatment.

Inhibition of Lung Metastases. The effects of **1** on lung metastasis formation were evaluated in mice carrying advanced MCa mammary carcinoma and compared to that of NAMI-A (Table 3). **1** markedly inhibited lung metastasis in mice bearing MCa mammary carcinoma; metastasis weight and number were reduced of 85% and 80%, respectively, in comparison to untreated controls. The effects on lung metastases are comparable to those caused by an equitoxic dose of NAMI-A. Reduction of primary tumor growth was irrelevant 24 h after the last compound administration, but it becomes statistically significant the day of metastasis evaluation.

Ruthenium Uptake by Primary Tumor and Host Tissues. The ruthenium uptake by primary tumor and by other host tissues such as blood, lungs, liver, and kidneys, taken from three mice of each group treated (**1** or NAMI-A), of the same experiment of Table 3, is reported in Figure 9. The greatest amount of **1** is found in kidneys and liver. The amount in tumor and lungs is approximately 50% of that measured in kidneys and liver. In blood, **1** is mainly in the plasma fraction (93% of the total amount present in the whole blood). The uptake of **1** by these tissues is comparable to that of NAMI-A, with the exception of lungs, in which the amount of **1** present is statistically lower than that of NAMI-A.

Histological Analysis. The histological analysis of liver sections from untreated mice evidenced hypoxic areas around the central veins, some dilated sinusoids, and some clusters of inflammatory cells in the parenchyma related to the advanced stage of tumor growth (see Supporting Information). Treatment with NAMI-A increased the number of dilated sinusoids and of the clusters of inflammatory cells. Hypoxic areas were more pronounced, hepatocytes appeared swollen and edematous, and small areas of necrotic cells were also present. The histological feature of livers of mice treated with **1** showed an even greater damage. The architecture of liver is seriously altered. The areas where liver cells are poorly stained and mummified (necrosis) are more extensive than those observed in animals treated with NAMI-A.

The histological features of kidneys, illustrated in Figure 10, show a normal architecture in all control animals, despite the presence of inflammatory processes around some vessels that determine dilation of adjacent tubules and, consequently, some damage to glomeruli. After treatment with NAMI-A, the whole parenchyma appeared seriously altered; tubules were edematous, some glomeruli had partially lost the definition of the Bowmann capsule, and others showed signs of atrophy or injury. Compound **1** caused less glomerular damages and tubule dilation than NAMI-A, even though the inflammatory processes were abundantly present and extensively widespread.

Discussion

Because of the relatively labile nature of many metal−ligand bonds, it is important to study the stability of metallodrugs under biologically relevant conditions. In particular, it is necessary to understand the hydrolysis properties of metal-based antitumor complexes because often the hydrolyzed species are the actual active metabolites in vivo causing the biological response finally leading to antitumor activity. Considering the hydrolytic processes of the NAMI(-A)-type

Table 3. Effects of **1** and NAMI-A on Lung Metastasis Formation in Mice with MCa Mammary Carcinoma[a]

compd (mg kg^{-1} day^{-1})[b]	primary tumor weight at day 16 (mg)	primary tumor weight at day 19 (mg)[c]	lung metastases	
			number[c]	weight[c]
controls	2515 ± 240	4297 ± 219	42.3 ± 4.7	126 ± 20.7
NAMI-A	2267 ± 223	2706 ± 131**	7.0 ± 1.5***	19.0 ± 5.20***
(35 × 6)	(90.1%)	(63.0%)	(16.5%)	(15.0%)
1	2149 ± 223	2562 ± 234**	8.4 ± 3.2***	18.2 ± 7.6***
(29 × 6)	(85.4%)	(59.6%)	(19.8%)	(14.4%)

[a] Groups of 10 CBA mice, inoculated im with 10^6 MCa tumor cells on day 0 were treated ip with the ruthenium complexes at the reported doses for 6 consecutive days, starting from day 10 to 15. Primary tumor growth was evaluated on day 16 or 19. Lung metastasis were determined on day 19. [b] The doses of NAMI-A and **1** administrated correspond to 77 and 47 μmol kg^{-1} day^{-1}. **1** is therefore administered at a lower dose than NAMI-A. Data in parentheses are expressed as the percentage of treated versus controls (*T*/*C*, %). [c] Statistical analysis includes ANOVA and the Tukey−Kramer post-test: (**) $p < 0.01$ and (***) $p < 0.001$ versus controls.

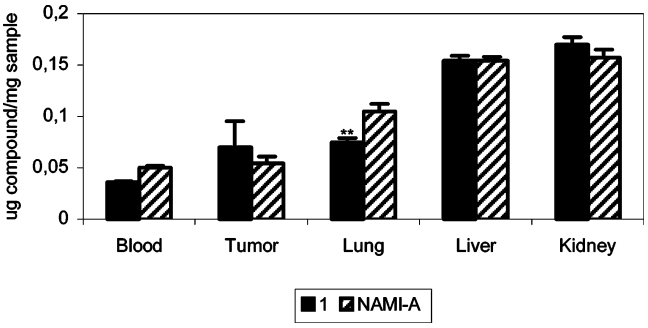

Figure 9. Ruthenium uptake by host tissue and primary tumor in mice with MCa mammary carcinoma. Three mice per group of the experiments reported in Table 3 were killed 24 h after the last drug administration, and primary tumor, liver, kidneys, lungs, and blood were harvested and processed for ruthenium determination by atomic absorption spectroscopy expressed as ruthenium concentration in each organ tested (μg/mg of wet tissue). Statistical analysis include ANOVA and the Tukey−Kramer post-test ((**) $p < 0.01$ vs NAMI-A).

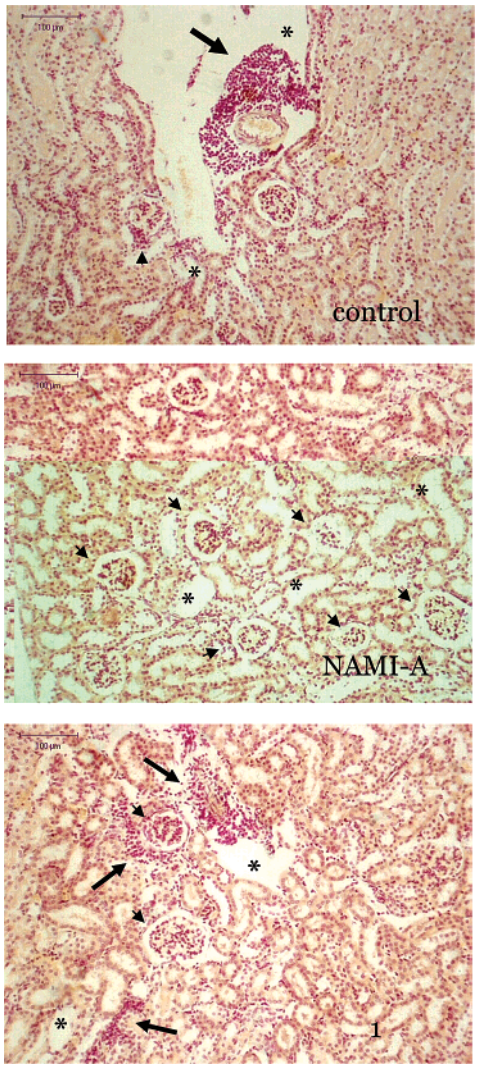

Figure 10. Histological analysis of kidneys injury (Cajal's trichrome, bar = 100 μm). Arrows show inflammatory process. Asterisks indicate enlarged tubules. Arrowheads show damaged glomeruli.

ruthenium complexes, it appears correct to consider them as prodrugs that rapidly undergo hydrolysis to form various aqua species in equilibrium with the corresponding hydroxo compounds in a pH-dependent manner.[19] The exact hydrolysis processes occurring are complicated to study, and they might also vary between the different NAMI(-A)-type complexes, depending on the nature of the nitrogen donor ligands.

According to UV−vis and NMR spectroscopies, in nonbuffered aqueous solutions NAMI-A and **1** behave differently. Compound **1**, in fact, shows a clear hydrolysis process that is concomitant with an increase of the acidity of the solution to pH ∼3 and formation of the neutral [*mer*-$RuCl_3(H_2O)$(dmso-S)(dmtp)]·H_2O compound **3**. The easy synthesis and isolation of the monoaqua complex **3** are favored by the intramolecular hydrogen-bonding properties of the dmtp with the coordinated water molecule.[21,23,29,30] At the slightly acidic pH, deprotonation of the coordinated water molecule is disfavored and consecutive loss of a second chloride ion is inhibited. Under similar conditions NAMI-A does not hydrolyze a chloride ion but actually slowly loses the coordinated dmso molecule, which is accompanied by a steady decrease of the main absorption band at ca. 400 nm.[19] For **1** or **2**, no loss of the coordinated dmso is observed. However, a detailed examination of the NMR and UV−vis data indicates that the first hydrolysis step of **1** and **2** is accompanied by a side process (see Figure 11), i.e., the partial release of the coordinated dmtp to form the [*trans*-$RuCl_4$(dmso-S)$(H_2O)]^-$ species, perhaps at equilibrium. It is known that at low pH this latter species undergoes the clean hydrolysis of one chloride to yield [*trans*-$RuCl_3$(dmso-S)$(H_2O)_2$], however, with a lower rate than that observed here.[13,24] We can conclude that chloride hydrolysis occurs mainly on [*trans*-$RuCl_4$(dmso-S)(dmtp)]$^-$ to form **3**, even though it is possible that dmtp might recoordinate to the bisaquaruthenium complex [*trans*-$RuCl_3$-(dmso-S)$(H_2O)_2$], stabilized by the intramolecular hydrogen bond with a water molecule (Figure 11). Besides

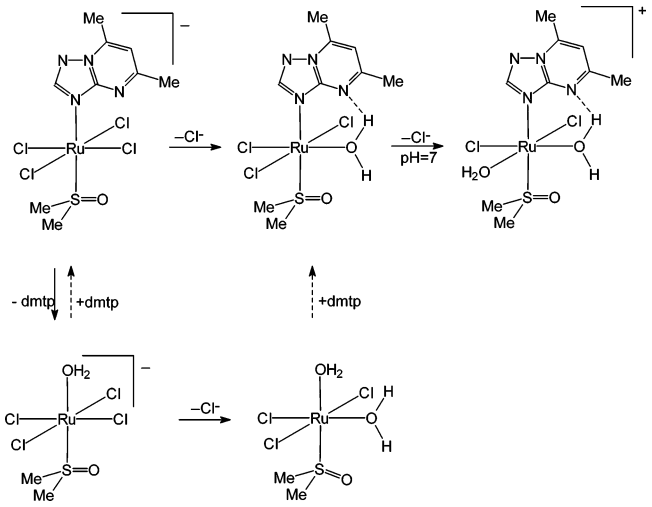

Figure 11. Hydrolysis scheme of the anion of **1** and **2**. In nonbuffered aqueous solutions, the hydrolysis of a chloride ion is observed, yielding the monoaqua complex **3.** However, the formation of **3** might also be achieved, at least in part, by a process involving the loss and recoordination of the dmtp ligand (dotted arrows). At physiological pH, the hydrolysis of a second chloride also occurs (even though the *cis*-diaquo complex is in the scheme, the geometry of the product is unknown), eventually followed by decomposition and formation of polymeric species.

being byproducts of the hydrolysis of **1** and **2**, [*trans*-$RuCl_4$(dmso-S)$(H_2O)]^-$ and [*trans*-$RuCl_3$(dmso-S)$(H_2O)_2$] are also the hydrolysis products of $(dmso_2H)$[*trans*-$RuCl_4$(dmso-S)$_2$]. The cytotoxicity and antitumor activity of the latter compound have been investigated in the early 1990s and are negligible;[35] therefore, the activity of **1** can be attributed to the activity of the compounds formed by hydrolysis of chloride ions, depicted in Figure 11, and not to the byproducts formed by partial hydrolysis of the heterocyclic ligand.

In contrast to the different behavior in nonbuffered aqueous solutions, the hydrolytic properties of **1** and **2** under physiological conditions are quite similar to those observed for the NAMI(-A) complex,[18,19] showing two consecutive hydrolysis steps in which chloride ions are hydrolyzed. Apparently, at physiological pH the coordinated water molecule of the first hydrolysis product, e.g., **3**, is easily deprotonated and the corresponding hydroxo complex can hydrolyze a further chloride. In contrast to what is observed in nonbuffered solutions, dissolution of **1** under physiological conditions does not seem to be accompanied by an initial increase of the Cl → Ru CT absorption, i.e., loss of the dmtp. However, these data are difficult to interpret because at pH 7.4 the first chloride hydrolysis is very fast, with a consequent decrease of the Cl → Ru CT absorption.

For NAMI-A, partial loss of the dmso molecule after dissolution in aqueous solutions is associated with increased kidney toxicity.[19] In contrast, **1** does not show this tendency to lose the coordinated dmso molecule and, interestingly, **1** shows a reduced kidney toxicity. However, under physiological conditions, **1** and NAMI-A appear to behave quite similarly, and therefore, it is too precocious to draw conclusions regarding a possible correlation between increased stability of the Ru−dmso bond and diminished kidney toxicity. However, the different physicochemical properties of NAMI-A-type complexes with different heterocyclic ligands together with the differences in biological activity (toxicity) might allow and strongly encourage the search for the structure−activity relationship (SAR) of this important class of antimetastatic complexes. Another advantageous aspect of increased Ru−dmso stability would be for the potential clinical formulation of NAMI-A-type drugs. Clearly, the stability of the dmso and the heterocyclic ligands are related to each other, as is obvious from the hydrolysis studies in nonbuffered aqueous solutions, and therefore requires a careful examination.

The above-described hydrolysis studies in buffered physiological solutions indicate that in the first hours after dissolution of **1** the biologically active metabolites are the first and second chloride hydrolysis products. Though the biological target of NAMI-A-type complexes is not known yet, nitrogen ligands present in proteins[36] or nucleic acids[37] are likely to coordinate to the ruthenium. Monoaquaruthenium(III) complexes are potential metabolic products for interacting with biological target molecules, as has been proven for the first hydrolysis product of the Keppler-type antitumor compounds.[25,30,38] The monoaqua complex **3** is therefore a useful starting compound for the further investigation of the in vivo reactions of NAMI-type antimetastasis drugs. In addition, the monoaqua complex **3** might be a useful starting compound for the synthesis of neutral trichlororuthenium(III) complexes.[25,34] In fact, the solvolysis studies of **3** in coordinating solvents (Solv) like dmso, DMF, and acetonitrile indicate the easy formation of complexes of the type [*mer*-$RuCl_3$(Solv)(dmso-S)(dmtp)].

Replacement of imidazole with dmtp does not modify the effect of NAMI-A-type complexes on solid tumor metastases. This result is in line with previous findings indicating that imidazole may be replaced by other heterocycles such as pyrazine and pyrazole.[39] The resulting molecules were as active as NAMI-A in vivo; in vitro they were devoid of effects on cell proliferation and on cell cycle but still had a marked effect on tumor cell invasion and on gelatinase activity. It thus seems that within the so-called NAMI-A-type compounds, changing the heterocyclic ligand is not determinant for in vivo activity although the stability of the molecule to hydrolysis, in particular in nonbuffered solutions, might be markedly different among the compounds of the group. Furthermore, these compounds have in common a low or absent in vitro cytotoxicity for tumor cells. The lack of in vitro cytotoxicity should not be attributable to methodological problems; i.e., NAMI-A needs to be metabolically activated to exert cytotoxicity. The need for metabolic activation should be ruled out because in vivo all these compounds showed a selective toxicity for metastatic cells and a common low efficacy on tumor cells at the primary site of growth. Rather, it might be stressed that these compounds modulate cancer growth by interacting with the processes responsible for tumor malignancy, showing a unique propensity to interact only with cells endowed with high metastasizing ability.[40] These cells represent only a small fraction of the whole burden of cells that constitute a tumor at the primary site of growth and do not represent the characteristics of in vitro cell lines, which only rarely induce spontaneous metastases after in vivo implantation in animals.

Conclusions

The NAMI-A analogue (Hdmtp)[*trans*-$RuCl_4$(dmso-S)(dmtp)], **1**, the related NAMI analogue (Na)[*trans*-$RuCl_4$(dmso-S)(dmtp)], **2**, and their first hydrolysis product [*mer*-$RuCl_3(H_2O)$(dmso-S)(dmtp)], **3**, were synthesized and characterized in solution as well as in the solid state. The hydrolysis properties of **1** and **2** were compared with those of the structurally similar antimetastatic compound NAMI-A. In nonbuffered aqueous solutions, in the first hours after dissolution the anionic compounds slowly hydrolyze a chloride ion to form the poorly soluble monoaqua complex **3** within hours at ambient temperature. Under physiological conditions the chloride hydrolysis is much faster (minutes) and it is followed by a second chloride hydrolysis step; these two hydrolysis products are the two most likely metabolites to exert biological activity in vitro and in vivo. The main differences with respect to NAMI-A are the increased stability of **1** in aqueous solutions with regard to loss of the coordinated dmso and the hydrolysis of a chloride under these conditions, favored by the hydrogen-bonding ability of the dmtp ligand.

The in vitro biological behavior of **1** is in some aspects different from that of NAMI-A, while the in vivo antimetastatic activity is of the same order of magnitude. The investigation of NAMI-A-type complexes therefore is most informative to tune and optimize the physicochemical properties of this class of antimetastatis complexes and to gain a better understanding of the mechanism of action. In particular, dmtp has proved to be a most useful ligand, first, because it allowed the isolation of the first $Ru-OH_2$ hydrolysis intermediate **3** owing to its hydrogen-bonding ability and, second, because of the pronounced biological activity of **1** despite its differences with NAMI-A regarding physicochemical properties and some in vitro tests. Furthermore, **3** promises to be a useful compound for SAR studies for further investigation of in vivo metabolites, as well as the interaction thereof with biological target molecules.

Experimental Section

Materials. The ligand dmtp[23,41] and the starting compounds (Na)[*trans*-$RuCl_4$(dmso-$S)_2$] and ($dmso_2$H)[*trans*-$RuCl_4$(dmso-$S)_2$][13,24] were prepared as described before. For the pharmacological and biological experiments, all chemicals were purchased from Sigma (St. Louis, MO) unless otherwise indicated. Trypsin-EDTA solution, MEM, MDEM, and RPMI 1640 medium for tumor cell lines as well as the used additives (Hank's salt, amino acids, sugars, antibiotics) were obtained from EuroClone (Wetherby, U.K.) except for fetal bovine serum (FBS), which was purchased from Invitrogen Italia (Milano, Italy). NAMI-A was prepared according to reported procedures.[42]

Instrumental Methods. Infrared spectra were recorded in KBr windows on a Perkin-Elmer 983G spectrometer. UV−vis spectra were obtained on a Jasco V-550 spectrometer. ^{1}H NMR spectra (ca. 1 mM samples) were recorded at 400 MHz on a JEOL Eclipse 400 FT instrument. All spectra were run at room temperature in D_2O or CD_2Cl_2. Proton peak positions were referenced to the peak of residual nondeuterated solvent. The paramagnetic ruthenium(III) complexes have been characterized using large spectral windows (12.000−50.000 Hz). Diamagnetic (solvent) sand paramagnetic signals were discriminated by using the inversion recovery pulse technique ($\pi-\tau-{}^1/_2\pi$ FID, with π and ${}^1/_2\pi$ the inversion, respectively, recording pulse and τ the inversion−recovery time),[43] using typical values for τ of about 50−100 ms.[25] The X-ray diffraction studies on the crystals of **1** and **3** were carried out on an Enraf-Nonius CAD4 diffractometer, equipped with graphite monochromator and Mo Kα radiation (λ = 0.710 73 Å). Unit cell dimensions were obtained from a least-squares fit of the setting angles of 25 reflections in the θ range 10.0−14.5°. Intensity data were corrected for Lorentz polarization effects and absorption through an empirical ψ-scan method. Both the structures were solved by conventional Patterson and Fourier techniques[44] and refined by a full-matrix anisotropic least-squares method.[44] A Fourier difference synthesis revealed the presence of a disordered diethyl ether molecule in **1**, (occupancy = 0.5, based on the Fourier peaks) and of a lattice water in **3**. All the calculations were performed using the WinGX System, version 1.64.02.[45]

Syntheses. Compounds **1** and **2** were prepared following the procedures described for NAMI-A and NAMI, respectively.[24,42] Compound **3** was prepared starting from compound **1** as well as from compound **2**, both syntheses resulting in the same product.

(Hdmtp)[*trans*-$RuCl_4$(dmso-S)(dmtp)], 1. A 0.31 g amount of ($dmso_2$H)[*trans*-$RuCl_4$(dmso-$S)_2$] (0.56 mmol) and 0.21 g of dmtp (1.4 mmol) were partially dissolved in 10 mL of acetone. The orange suspension was stirred for 6 h at room temperature and then filtered; the residue was washed with cold acetone and diethyl ether and dried in vacuo. Yield was 0.28 g (80%). Crystals suitable for XRD analyses were grown by diethyl ether diffusion into a concentrated solution of **1** in dichloromethane. Anal. ($C_{16}H_{23}N_8Cl_4ORuS\cdot{}^1/_4(CH_3CH_2)_2O$) C, H, N. ^{1}H NMR (300 MHz, 20 °C, dichloromethane-d_2): δ −0.72 (broad, 3H), 0.87 (broad, 3H), 4.14 (broad, 1H), all dmtp; −14.6 (very broad, 6H), dmso-S; 2.07 (s, 3H), 2.85 (s, 3H), 7.54 (s, 1H), all Hdmtp signals. ^{1}H NMR (300 MHz, 20 °C, D_2O, fresh): δ −0.59 (broad, 3H), 1.37 (broad, 3H), dmtp; −14.6 (very broad, 6H), dmso-S; 2.53 (s, 3H), 2.66 (s, 3H), 7.09 (s, 1H), 8.44 (s, 1H), (H)dmtp signals. IR data, cm^{-1}: 3000 (br), 1647 (vs), 1626 (vs), 1090 (s), 431 (w), and 337 (m). Crystal data: $C_{17}H_{25.50}Cl_4N_8O_{1.25}RuS$, M = 636.88, tetragonal, space group $P\bar{4}2_1c$, a = 19.931(2) Å, c = 14.070(2) Å, V = 5589.5(12) Å^3, Z = 8, ρ_{calcd} = 1.514 g/cm^3, μ(Mo Kα) = 1.044 mm^{-1}, F(000) = 2572. Final R = 0.0467, wR2 = 0.1229, S = 1.068 for 290 parameters and 6542 reflections, 3339 unique [R(int) = 0.0550], of which 2269 have $I > 2\sigma(I)$, max positive and negative peaks in ΔF map 0.866, −0.461 e Å^{-3}.

(Na)[*trans*-$RuCl_4$(dmso-S)(dmtp)], 2. An amount of 0.15 g of (Na)[*trans*-$RuCl_4$(dmso-$S)_2$] (0.35 mmol), dissolved in 8 mL of acetone and 2 mL of dmso, and 0.15 g of dmtp (1 mmol), dissolved in 10 mL of acetone, were stirred for 7 h at room temperature. The suspension was filtered, and the residue was extensively washed with cold acetone and diethyl ether and dried in vacuo. Yield was 0.13 g (75%). Anal. ($C_9H_{14}N_4Cl_4$-NaORuS) C, H, N. ^{1}H NMR data (in D_2O) are the same as for **1** except for the Hdmtp signals of the counterion. For the IR data of **2**, the ruthenium−ligand and dmso vibrations of **2** are the same as those observed for **1**. In contrast to **1**, only one set of dmtp vibrations is observed because the vibrations of the protonated dmtp, present in the latter but not in **2**, are absent.

[*mer*-$RuCl_3(H_2O)$(dmso-S)(dmtp)]·H_2O, 3. This compound was prepared in two ways. (1) An amount of 60 mg of **1** was dissolved in 6 mL of water. After 1 day, in the light-orange solution (pH ∼2) yellow-brown crystals were found. They were filtered off, washed with water, ethanol/diethyl ether (1/5), and diethyl ether, and air-dried. Yield was 10 mg (20%). (2) An amount of 50 mg of **2** was dissolved in 10 mL of water. On standing at room temperature, the solution gradually turned from light-orange to green and, after 2 days, brown crystals started depositing. At this time the pH of the solution had lowered to about pH ∼3. The crystalline material was filtered off and washed as described above. Yield was 10 mg (20%). The elemental analyses and the IR, ^{1}H NMR, and UV−vis absorption data of the compounds obtained from both synthetic routes are identical. Anal. ($C_9H_{18}N_4Cl_3RuO_3S$) C, H, N. ^{1}H NMR (300 MHz, 20 °C, dichloromethane-d_2): δ −0.17 (broad, 3H), 1.55 (broad, 3H), 4.91 (broad, 1H), all dmtp; −14.3 (very broad, 6H), dmso-S. IR data, cm^{-1}: 3488 (s), 3395 (s),

3000 (s, broad), 1623 (vs), 576 (w), 429 (w), 341 (m). Crystal data: $C_9H_{18}Cl_3N_4O_3RuS$, $M = 469.75$, monoclinic, space group $P2_1/n$, $a = 11.586(1)$ Å, $b = 11.000(1)$ Å, $c = 14.214(2)$ Å, $\beta = 109.42(1)°$, $V = 1708.5(3)$ Å^3, $Z = 4$, $\rho_{calcd} = 1.826$ g/cm^3, μ(Mo Kα) = 1.521 mm^{-1}, $F(000) = 940$. Final $R = 0.0282$, wR2 = 0.0720, $S = 1.102$ for 205 parameters and 5142 unique reflections, of which 4348 have $I > 2\sigma(I)$, max positive and negative peaks in ΔF map 0.334, −0.850 e Å^{-3}.

Tumor Lines for in Vitro Tests. The B16-F10 murine melanoma cell line was obtained from ATCC (Manassas, VA), catalog number CRL-6475. Cells were cultured in minimal essential medium (MEM) with Hank's salts adjusted to contain 1.5 g/L sodium bicarbonate, 4.5 g/L glucose, 1 mM sodium pyruvate, 10% FBS, 2 mM L-glutamine, 100 U/mL penicillin, 100 μg/mL streptomycin solution, and 1% nonessential amino acids.

TS/A murine adenocarcinoma cell line was originally obtained by Dr. G. Forni (Consiglio Nazionale delle Ricerche, Centro di Immunogenetica ed Oncologia Sperimentale, Torino, Italy). Cells were cultured, according to standard procedure,[46] in RPMI 1640 medium supplemented with 10% FBS, 2 mM L-glutamine, and 50 μg/mL gentamicin sulfate.

The KB human oral carcinoma cell line was obtained from ECACC, catalog number 86103004. Cells were cultured in minimal essential medium (MEM) with Hank's salts adjusted to contain 1.5 g/L sodium bicarbonate, 10% FBS, 2 mM L-glutamine, 100 U/mL penicillin, 100 μg/mL streptomycin solution, 1 mM sodium pyruvate, 1% nonessential amino acids, and 1 mM HEPES solution.

HT1080 human fibrosarcoma cell line was originally obtained by Dr. S. Garbisa (Istituto di Istologia ed Embriologia Generale, University of Padua, Italy). Cells were maintained in DMEM with 10% FBS, 2 mM L-glutamine, 100 U/mL penicillin, and 100 μg/mL streptomycin solution.

All cell lines were kept in a CO_2 incubator with 5% CO_2 and 100% relative humidity at 37 °C. Cells from a confluent monolayer were removed from flasks by a trypsin−EDTA solution. Cell viability was determined by the trypan blue dye exclusion test. For experimental purposes, cells were sown in multiwell cell culture clusters.

In Vitro Cytotoxicity Evaluation. Cell growth was determined by MTT assay.[47] Cells were sown on 96-well plates (Corning Costar Italia, Milano, Italy) and 24 h after sowing were incubated with compounds at 1−100 μM, prepared by dissolving in an appropriate medium containing 5% of serum for 24 or 72 h. Analysis was performed at the end of the incubation time. Briefly, MTT dissolved in PBS at 5 mg/mL was added (10 μL per 100 μL of medium) to all wells and plates were incubated at 37 °C for 4 h. At the end of the incubation, the medium was discarded and 100 μL of acidified 2-propanol (0.2 mL of 0.04 N HCl in 10 mL of 2-propanol) was added to each well according to the modification used by Galeano et al.[11] Optical density was measured at 570 nm on a Spectra-Count Packard (Meriden, CT) instrument.

Invasion Assay. Invasive capability was measured in a transwell cell culture chamber (Corning Costar Italia, Milano, Italy) according to a method modified from Albini.[48] In brief, the surface of a poly(vinylpyrrolidone)-free polycarbonate filter (6.5 mm diameter and 8 μm pore size) was coated with 30 μg/50 μL of matrigel (Beckton Dickinson, Bedford, MA) diluted in RPMI-1640 and air-dried overnight at room temperature. The filters were reconstituted with RPMI-1640 medium immediately before use. TS/A adenocarcinoma cells were treated for 1 h with **1** at 100 μM in PBS Ca^{2+}−Mg^{2+} saline solution. At the end of the treatment, cells were harvested with trypsin−EDTA, counted, and resuspended and 1×10^5 cells were sowed in 100 μL of complete medium in the upper compartment chamber, in triplicate. The lower compartment was filled with RPMI-1640, supplemented with 10% FBS, 2 mM L-glutamine, and 50 μg/mL gentamicine sulfate solution. Plates were left in the incubator for 96 h at 37 °C, 5% CO_2, and 100% relative humidity. At the end of the incubation, the cells that had migrated from the upper to the lower side of the chamber were detached with trypsin−EDTA and the cell number was determined. The invasion is expressed as the percent ratio of the number of invading cells (lower well sample) to the total number of cells sown in the upper well sample.

Evaluation of the Inhibition of Gelatinase Activity. To visualize the direct effect of the **1** on MMP-9 enzyme, an SDS−PAGE zymography was carried out with a conditioned medium of fibrosarcoma HT-1080 cells. The conditioned medium was prepared by incubating subconfluent cells with serum-free medium overnight. The supernatant was collected and centrifuged to remove cellular debris and concentrated 20 times by centrifugation using Millipore AMICON HM-10 ultracentrifugation tubes (Millipore Corporation, Bedford, MA).The conditioned medium obtained was stored at −20 °C until use. The samples were eluted with Laemmli sample buffer and analyzed by SDS−PAGE on a 7% polyacrilamide gel containing 0.1% (w/v) gelatin. At the end of electrophoresis in a dual laboratory system (Protean II, Bio-Rad Laboratories, Hercules CA), gels were washed twice for 30 min at 4 °C in 2.5% Triton X-100 to remove SDS. After additional washings in water (three times, 5 min to remove Triton X-100), the gels were cut into strips and incubated with different concentrations of **1** (0−2.67 mM) for 30 min at 4 °C and then for 18 h at 37 °C. The incubation with compounds was performed in collagenasis buffer (200 mM NaCl, 50 mM Tris, 10 mM $CaCl_2$, adjusted to pH 7.4), and 10 mM EDTA was used as a positive control. The gels strips were then stained with 0.5% Coomassie brilliant blue. The gelatinolytic regions were observed as white bands against a blue background. MMP activity was measured by scoring the intensity of bands by computerized image analysis (Apple Computer Inc., Cupertino, CA).

Cell Cycle Analysis. Viable cells (0.5×10^6) of a single cell suspension were fixed in 70% ethanol at 4 °C for at least 1 h. Before analysis, the ethanol was removed by centrifugation and cells were washed twice with PBS. Cells were resuspended in PBS containing 1 mg/mL RNase at 37 °C for 30 min and further stained for at least 30 min at room temperature in the dark with propidium iodide (40 μg/mL) (modified from Crissman[49]). Red fluorescence (610 nm) was analyzed using a peak fluorescence gate to discriminate aggregates. Each analysis consisted of 10 000 events counted. The flow cytometry analyses were done with an EPICS XL flow cytometer (Coulter Electronics, Miami, FL). Cell cycle distribution of the cells was determined by analysis with Multicycle software (Phoenix Flow Systems, San Diego, CA).

Tumor Cell Line for in Vivo Test. The MCa mammary carcinoma line of CBA mouse was originally obtained from Rudjer Boskovic Institute, Zagreb, Croatia.[50] Tumor lines were locally maintained by serial biweekly passages of 10^6 viable tumor cells, obtained from donors similarly inoculated 2 weeks before, and injected im (intramuscularly) into the calf of the left hind leg of CBA adult mice. Tumor propagation for experimental purposes was similarly made using CBA mice obtained from a locally established breeding colony, grown according to the standard procedure for inbred strains. Briefly, 2.5 g of freshly removed tumor was minced with scissors, finely dispersed in Dulbecco's phosphate buffer saline, Ca^{2+}- and Mg^{2+}-free (PBS), and filtered through a double layer of sterile gauze. After centrifugation at 250*g* for 10 min, pellets were resuspended in an equal volume of PBS and cell viability was checked by the trypan-blue exclusion test; only cell suspensions with at least 55−60% viable cells were used.

In Vivo Treatments. For in vivo studies compounds were dissolved in isotonic nonpyrogenic physiological saline. NAMI-A and **1** were given to mice by ip (intraperitoneal) administration of 35 mg kg^{-1} day^{-1} (77 μmol kg^{-1} day^{-1}) and 29 mg kg^{-1} day^{-1} (47 μmol kg^{-1} day^{-1}), respectively, in a volume of 0.1 mL/10 g of body weight. The doses used correspond to the $LD_{0.05}$ of each compound previously calculated in toxicity experiments. Treatment was performed daily for 6 consecutive days starting when the primary tumor was visible.

Primary Tumor Growth and Lung Metastasis Evaluation. Primary tumor growth was determined by calliper measurements by determining two orthogonal axes and calculating tumor volume with the formula $(\pi/6)a^2b$ ($a < b$) and

assuming tumor density equal to 1. The evaluation of the number and weight of lung metastases, spontaneously formed from the im tumor implants, was performed at about 3 weeks from tumor implantation after sacrificing the animals by cervical dislocation. The number of lung colonies were counted by carefully examining the surface of the lungs, which were dissected into five lobes, washed with PBS, and examined under a low-power microscope equipped with a calibrated grid. The weight of each metastatic nodule was calculated by applying the same formula used for primary tumors; the sum of these individual weights gives the total weight of the metastatic tumor per animal.

Animal Studies. Animal studies were carried out according to the guidelines in force in Italy (guideline DDL 116 of Februrary 21, 1992) and in compliance with the Guide for Care and Use of Laboratory Animals, Department of Health and Human Services Publication No. (NIH) 86-23, Bethesda, MD, National Institutes of Health, 1985.

Ruthenium Uptake Measurement. Twenty-four hours after the last drug administration blood, small pieces of primary tumor, or the whole organ (liver, kidney, lung), were carefully removed from three mice per group of treatment. A fragment of each organ specimen was carefully weighed and then dried overnight at 80 °C in a Nalgene cryogenic vial. In the second step, the samples were dried at 105 °C until they reached a constant dried weight. The decomposition of the dried organs was carried out according to a modification of the procedures by Tamura and Arai,[51] with the addition of an aliquot of tetramethylammonium hydroxide (TMAH, Aldrich Chimica, Milano, Italy) at 25% in water and an aliquot of MilliQ water at a ratio of 1:1 directly in the vial, at room temperature and under agitation. The final volumes were adjusted at 1 mL with MilliQ water. The concentration of ruthenium was measured in triplicate by means of graphite furnace atomic absorption spectrometry (GFAAS). The GFAAS instrument used was a graphite tube atomizer, model SpectrAA-220Z, and the power was supplied with a GTA 110Z unit equipped with a specific ruthenium emission lamp (hollow cathode lamp P/N 56-101447-00) (Varian, Mulgrave, Victoria, Australia). The lower and higher limits of quantitation (LLQ, HLQ) were set at the concentration levels that correspond respectively to the lowest and higher standard concentration. The limit of detection (LOD) was estimated according to the EURACHEM guide. The fitness was for the purpose of analytical methods. LLQ, HLQ, and LOD for Ru were respectively 20, 100, and about 10 ng mL^{-1}. The quantification of ruthenium was carried out in 10 μL samples at 349.9 nm with an atomizing temperature of 2.500 °C, using argon as the purge gas at a flow rate of 3.0 l min^{-1}. Before each daily analysis session, a five-point calibration curve was obtained using ruthenium, Custon-Grade Standard, 998 mg mL^{-1} (Inorganic Ventures Inc., Lakewood, NJ).

Histological Examination. Liver and kidneys of three different mice per group were removed from animals 24 h after the last drug administration, fixed in 10% formaline, and processed according to the standard procedure for inclusion and rehydration. Sections were cut at 6 μm, stained by Cajal's trichrome, and mounted in Canada Balsam. The histological analysis was performed by a Leitz Orthoplan microscope, and the images were acquired using the software Windows μImage, version 3.4 (Casti imaging, Venice, Italy).

Statistical Analysis. Data were submitted to computer-assisted statistical analysis using ANOVA (analysis of variance) and Dunnett's multiple-comparison test or Tukey–Kramer post-test.

Acknowledgment. Grant COST D8 was used for financial support of a short-term scientific mission of A.H.V. at University of Trieste. Prof. J. Reedijk (Leiden Institute of Chemistry) is acknowledged for reading a preliminary version of part of this manuscript. This work was supported in part by the Council for Chemical Sciences of The Netherlands Organization for Scientific Research (CS-NWO). Funding was from LINFA Laboratories and MURST "Meccanismi farmacologici dell'attività antimetastatica di farmaci basati su metalli" (Grant 2001053898-004).

Supporting Information Available: Crystal packing with hydrogen-bonding structure of **3**, ^{1}H NMR spectrum of **1** in CD_2Cl_2, UV–vis absorption spectra of **1** (followed in time) and **3** under physiological conditions, discussion of IR data of **1**–**3**, and histological analysis of sections of liver. This material is available free of charge via the Internet at http://pubs.acs.org.

References

(1) Clarke, M. J. Ruthenium metallopharmaceuticals. *Coord. Chem. Rev.* **2003**, *236*, 209–233.
(2) Clarke, M. J.; Zhu, F.; Frasca, D. R. Non-Platinum Chemotherapeutic Metallopharmaceuticals. *Chem. Rev.* **1999**, *99*, 2511–2533.
(3) Keppler, B. K. Metal complexes as anticancer agents. *New J. Chem.* **1990**, *14*, 389.
(4) Keppler, B. K.; Henn, M.; Juhl, U. M.; Berger, M. R.; Niebl, R.; Wagner, F. E. New Ruthenium Complexes for the Treatment of Cancer. *Prog. Clin. Biochem. Med.* **1989**, *10*, 42–69.
(5) Aird, R. E.; Cummings, J.; Ritchie, A. A.; Muir, M.; Morris, R. E.; Chen, H.; Sadler, P. J. In vitro and in vivo activity and cross resistance profiles of novel ruthenium(II) organometallic arene complexes in human ovarian cancer. *Br. J. Cancer* **2002**, *86*, 1652–1657.
(6) Morris, R. E.; Aird, R. E.; Murdoch, P. d. S.; Chen, H.; Cummings, J.; Hughes, N. D.; Parsons, S.; Parkin, A.; Boyd, G.; Jodrell, D. I.; Sadler, P. J. Inhibition of cancer cell growth by ruthenium(II) arene complexes. *J. Med. Chem.* **2001**, *44*, 3616–3621.
(7) Hotze, A. C. G.; Bacac, M.; Velders, A. H.; Jansen, B. A. J.; Kooijman, H.; Spek, A. L.; Haasnoot, J. G.; Reedijk, J. New cytotoxic and water-soluble bis(2-phenylazopyridine)ruthenium(II) complexes. *J. Med. Chem.* **2003**, *46*, 1743–1750.
(8) Velders, A. H.; Kooijman, H.; Spek, A. L.; Haasnoot, J. G.; De Vos, D.; Reedijk, J. Strong differences in the in vitro cytotoxicity of three isomeric dichlorobis(2-phenylazopyridine)ruthenium(II) complexes. *Inorg. Chem.* **2000**, *39*, 2966–2967.
(9) Depenbrock, H.; Schmelcher, S.; Peter, R.; Keppler, B. K.; Weirich, G.; Block, T.; Rastetter, J.; Hanauske, A.-R. Preclinical activity of *trans*-indazolium[tetracholorbisindazoleruthenate-(III)] (NSC 666158; IndCR.; KP 1019) against tumour colony-forming units and haematopoietic progenitor cells. *Eur. J. Cancer* **1997**, *33*, 2404–2410.
(10) Keppler, B. K.; Lipponer, K. G.; Stenzel, B. New Tumor-Inhibiting Ruthenium Complexes. *Metal Complexes in Cancer Chemotherapy*; VCH: Weinheim, Germany, 1993; pp 187–220.
(11) Galeano, A.; Berger, M. R.; Keppler, B. K. Antitumor activity of some ruthenium derivatives in human colon cancer cell lines in vitro. *Arzneim.-Forsch.* **1992**, *42*, 821–824.
(12) Sava, G.; Capozzi, I.; Clerici, K.; Gagliardi, R.; Alessio, E.; Mestroni, G. Pharmacological control of lung metastases of solid tumours by a novel ruthenium complex. *Clin. Exp. Metastasis* **1998**, 371–379.
(13) Alessio, E.; Balducci, G.; Lutman, A.; Mestroni, G.; Calligaris, M.; Attia, W. M. Synthesis and characterization of 2 new classes of ruthenium(III)–sulfoxide complexes with nitrogen donor ligands (L)–Na[*trans*-$RuCl_4(R_2SO)(L)$] and *mer*,*cis*-$RuCl_3(R_2SO)(R_2SO)(L)$–the crystal-structure of Na[*trans*-$RuCl_4$(DMSO)(NH_3)]·2DMSO, Na[*trans*-$RuCl_4$(DMSO)(Im)]·H_2O,Me_2CO (Im = imidazole) and *mer*,*cis*-$RuCl_3$(DMSO)(DMSO)(NH_3). *Inorg. Chim. Acta* **1993**, *203*, 205–217.
(14) Sava, G.; Alessio, E.; Bergamo, A.; Mestroni, G. Sulfoxide ruthenium complexes: non-toxic tools for the selective treatment of solid tumour metastases. *Topics in Biological Inorganic Chemistry*; Springer-Verlag GmbH & Co.: Berlin, 1999; pp 143–169.
(15) Sava, G.; Clerici, K.; Capozzi, I.; Cocchietto, M.; Gagliardi, R.; Alessio, E.; Mestroni, G.; Perbellini, A. Reduction of lung metastasis by ImH[*trans*-$RuCl_4$(DMSO)Im]: mechanism of the selective action investigated on mouse tumors. *Anti-Cancer Drugs* **1999**, *10*, 129–138.
(16) Sava, G.; Gagliardi, R.; Bergamo, A.; Alessio, E.; Mestroni, G. Treatment of metastases of solid mouse tumours by NAMI-A: Comparison with cisplatin, cyclophosphamide and dacarbazine. *Anticancer Res.* **1999**, *19*, 969.
(17) Schellens, J. H. M. Personal communication to G. Sava, 2002.
(18) Mestroni, G.; Alessio, E.; Sava, G.; Pacor, S.; Coluccia, M.; Bocarelli, A. Water soluble ruthenium(III)–dimethylsulfoxide complexes: chemical behaviour and pharmaceutical properties. *Met.-Based Drugs* **1993**, *1*, 41–63.

(19) Sava, G.; Bergamo, A.; Zorzet, S.; Gava, B.; Casarsa, C.; Cocchietto, M.; Furlani, A.; Scarcia, V.; Serli, B.; Iengo, E.; Alessio, E.; Mestroni, G. Influence of chemical stability on the activity of the antimetastasis ruthenium compound NAMI-A. *Eur. J. Cancer* **2002**, *38*, 427−435.
(20) Bouma, M.; Nuijen, B.; Jansen, M. T.; Sava, G.; Flaibani, A.; Bult, A.; Beijnen, J. A kinetic study of the chemical stability of the antimetastatic ruthenium complex NAMI-A. *Int. J. Pharm.* **2002**, *248*, 239−246.
(21) Salas, J. M.; Romero, M. A.; Sanchez, M. P.; Quiros, M. Metal complexes of [1,2,4]triazolo-[1,5-*a*]pyrimidine derivatives. *Coord. Chem. Rev.* **1999**, *195*, 1119.
(22) Haasnoot, J. G. Mononuclear, oligonuclear and polynuclear metal coordination compounds with 1,2,4-triazole derivatives as ligands. *Coord. Chem. Rev.* **2000**, *200*−*202*, 131−185.
(23) Velders, A. H.; Pazderski, L.; Ugozzoli, F.; Biagini-Cingi, M.; Manotti-Lanfredi, A. M.; Haasnoot, J. G.; Reedijk, J. Synthesis, characterization and crystal structure of trans-aquatrichlorobis (5,7-dimethyl[1,2,4]triazolo[1,5-*a*]pyrimidine-N-3)ruthenium-(III) monohydrate. *Inorg. Chim. Acta* **1998**, *273*, 259−265.
(24) Alessio, E.; Balducci, G.; Calligaris, M.; Costa, G.; Attia, W. M.; Mestroni, G. Synthesis, molecular-structure, and chemical behavior of hydrogen *trans*-bis(dimethyl sulfoxide)tetrachlororuthenate(III) and *mer*-trichlorotris(dimethyl sulfoxide)ruthenium-(III)−the 1st fully characterized chloride dimethyl-sulfoxide ruthenium(III) complexes. *Inorg. Chem.* **1991**, *30*, 609−618.
(25) Velders, A. H. Ruthenium complexes with heterocyclic nitrogen ligands. Ph.D. Thesis, Leiden University, Leiden, The Netherlands, 2000; p 288.
(26) Turel, I.; Pecanac, M.; Golobic, A.; Alessio, E.; Serli, B. Novel Ru-(III)−dmso complexes of the antiherpes drug acyclovir. *Eur. J. Inorg. Chem.* **2002**, 1928−1931.
(27) Taqui Khan, M. M.; Ramachandraiah, G.; Shukla, R. S. Ruthenium(III) chloride in aqueous solution: kinetics of the aquation and anation reactions of the chloro complexes. *Inorg. Chem.* **1988**, *27*, 3274−3278.
(28) Price, C.; Shipman, M. A.; Gummerson, S. L.; Houlton, A.; Clegg, W.; Elsegood, M. R. J. Ruthenium−carbon bond formation via cyclometallation of a nucleobase. *J. Chem. Soc., Dalton Trans.* **2001**, 353−354.
(29) Velders, A. H.; Ugozzoli, F.; Biagini-Cingi, M.; Manotti-Lanfredi, A. M.; Haasnoot, J. G.; Reedijk, J. A unique fourfold intramolecular hydrogen bonding stabilises the structure of trans-bis-(2-amino-5,7-dimethyl[1,2,4]triazolo[1,5-alpha]pyrimidine-N-3)-aquatrichlororuthenium(III) monohydrate. *Eur. J. Inorg. Chem.* **1999**, 213−215.
(30) Velders, A. H.; Van der Geest, B.; Kooijman, H.; Spek, A. L.; Haasnoot, J. G.; Reedijk, J. Ruthenium(III) coordination to the exocyclic nitrogen of 9-methyladenine and stabilisation of the rare imine tautomer by intramolecular hydrogen bonding. *Eur. J. Inorg. Chem.* **2001**, 369−372.
(31) Alessio, E.; Mestroni, G.; Zangrando, E. Unpublished results.
(32) Duff, C. M.; Heath, G. A. From (RuX6) to (Ru(RCN)6): Synthesis of Mixed Halide−Nitrile Complexes of Ruthenium, and Their Spectroelectrochemical Characterization in Multiple Oxidation States. *J. Chem. Soc., Dalton Trans.* **1991**, 2401−2411.
(33) Turel, I.; Alessio, E. Unpublished results.
(34) Velders, A. H. Unpublished results.
(35) Bergamo, A.; Sava, G.; Alessio, E. Unpublished results.
(36) Messori, L.; Orioli, P.; Vullo, D.; Alessio, E.; Iengo, E. A spectroscopic study of the reaction of NAMI, a novel ruthenium-(III) anti-neoplastic complex, with bovine serum albumin. *Eur. J. Biochem.* **2000**, *267*, 1206−1213.
(37) Messori, L.; Casini, A.; Vullo, D.; Haroutiunian, S. G.; Dalian, E. B.; Orioli, P. Effects of two representative antitumor ruthenium(III) complexes on thermal denaturation profiles of DNA. *Inorg. Chim. Acta* **2000**, *303*, 283−286.
(38) Ni Dhubhghaill, O. M.; Hagen, W. R.; Keppler, B. K.; Lipponer, K.-G.; Sadler, P. J. Aquation of the Anticancer Complex trans-[Ru(III)Cl4(Him)2]- (Him = imidazole). *J. Chem. Soc., Dalton Trans.* **1994**, 3305.
(39) Bergamo, A.; Gava, B.; Alessio, E.; Mestroni, G.; Serli, B.; Cocchietto, M.; Zorzet, S.; Sava, G. Ruthenium-based NAMI-A type complexes with in vivo selective metastasis reduction and in vitro invasion inhibition unrelated to cell cytotoxicity. *Int. J. Oncol.* **2002**, *21*, 1331−1338.
(40) Sava, G.; Zorzet, S.; Turrin, C.; Vita, F.; Soranzo, M. R.; Zabucchi, G.; Cocchietto, M.; Bergamo, A.; DiGiovine, S.; Pezzoni, G.; Sartor, L.; Garbisa, S. Dual action of NAMI-A in inhibition of solid tumor metastasis: selective targeting of metastatic cells and binding to collagen. *Clin. Cancer Res.* **2003**, *9*, 1898−1905.
(41) Bülow, C.; Haas, K. Synthetische versuche zur darstellung von derivaten des heterokondensierten, heterocyclischen 1.3-triazo-7,0′-pyrimidins (Synthesis procedures for the preparation of derivatives of the heterocondensed, heterocyclic 1.3-triazo-7,0′-pyrimidines). *Ber. Dtsch. Chem. Ges.* **1909**, *42*, 4638−4644.
(42) Mestroni, G.; Alessio, E.; Sava, G. New salts of anion complexes of Ru(III) as antimetastatic and anti neoplastic agents. International Patent PCT C 07F 15/00, A61K 31/28, WO 98/00431, 1998.
(43) Friebolin, H. *Basic One- and Two-Dimensional NMR Spectroscopy*; VCH: Weinheim, Germany, 1991.
(44) Sheldrick, G. M. *SHELX97 Programs for Crystal Structure Analysis*, release 97-2; University of Göttingen: Göttingen, Germany, 1998.
(45) Farrugia, L. J. WinGX Suite for Single Crystal Small Molecule Crystallography. *J. Appl. Crystallogr.* **1999**, *32*, 837−838.
(46) Nanni, P.; De Giovanni, C.; Lollini, P. L.; Nicoletti, G.; Prodi, G. TS/A: a new metastasising cell line from BALB/c spontaneous mammary adenocarcinoma. *Clin. Exp. Metastasis* **1983**, *1*, 373−385.
(47) Mosmann, T. Rapid colorimetric assay for cellular growth and survival: application to proliferation and cytotoxicity assays. *J. Immunol. Methods* **1983**, *65*, 55−63.
(48) Albini, A.; Iwamoto, Y.; Kleinman, H. K.; Martin, G. R.; Aaronson, S. A.; Kozlowski, J. M.; McEwan, R. N. A rapid in vitro assay for quantitating the invasive potential of tumour cells. *Cancer Res.* **1987**, *47*, 3239−3245.
(49) Crissman, H. A.; Steinkamp, J. A. Rapid simultaneous measurement of DNA, protein and cell volume in single cells from large mammalian populations. *J. Cell Biol.* **1973**, *59*, 766−771.
(50) Poliak-Blazi, M.; Boranic, M.; Marzan, B.; Radacic, M. A transplantable aplastic mammary carcinoma of CBA mice. *Vet. Arh.* **1981**, *51*, 99−107.
(51) Tamura, H.; Arai, T. Determination of ruthenium in biological tissue by graphite furnace AAS after decomposition of the sample by tetramethylammonium hydroxide. *Bunseki Kagaku* **1992**, *41*, 13−17.

JM030984D